

Short- and medium-range order in amorphous Zr₂Ni metallic alloyLi Huang,¹ C. Z. Wang,^{1,2} S. G. Hao,¹ M. J. Kramer,^{1,3} and K. M. Ho^{1,2}¹*Ames Laboratory, U.S. Department of Energy, Ames, Iowa 50011, USA*²*Department of Physics, Iowa State University, Ames, Iowa 50011, USA*³*Department of Materials Science and Engineering, Iowa State University, Ames, Iowa 50011, USA*

(Received 6 November 2009; revised manuscript received 17 February 2010; published 30 March 2010)

Icosahedral clusters are commonly believed to be the key building blocks in many metallic glasses. Here we propose a structural model for Zr₂Ni metallic glass which has a small fraction of icosahedral clusters. By analyzing the correlation between the local structure and dynamics in the undercooled liquid and glass, we show that the formation of metallic glass in this system can be attributed to the slow dynamics of $\langle 0,2,8,1 \rangle$ and $\langle 0,2,8,2 \rangle$ Ni-centered Voronoi polyhedra. There is a high proportion of less mobile $\langle 0,2,8,4 \rangle$, $\langle 0,2,8,5 \rangle$, $\langle 0,1,10,4 \rangle$, and $\langle 0,1,10,3 \rangle$ Zr-centered clusters on the first shell of the two types of Ni-centered clusters. These special Ni- and Zr-centered clusters arrange together to form a stringlike backbone network in the metallic glass.

DOI: [10.1103/PhysRevB.81.094118](https://doi.org/10.1103/PhysRevB.81.094118)

PACS number(s): 61.43.Dq, 61.05.C-, 31.15.A-, 61.20.Ja

I. INTRODUCTION

Describing the structure of metallic glasses has been a long-standing challenge in materials science.^{1–6} Recently, there has been increased recognition that structures of metallic glasses are better described by packing of clusters that have different local order characters.^{7–10} In particular, the 13-atom icosahedral cluster has been suggested as local structural unit responsible for the formation of metallic glasses.^{11–15} However, for some amorphous alloys, e.g., Zr₂Ni, it has been shown that the degree of icosahedral order is very small and unlikely to play a significant role in the glass formation in this system.^{16–22} Although this alloy has been a recent subject of numerous experimental^{16–20} and computational investigations,^{21,22} the short-range order (SRO) responsible for the glass formability and the nature of medium-range order (MRO) in this system is still a subject of debate. Saida *et al.*²³ and Liu *et al.*²⁴ suggested that the bond-length similarities in the amorphous Zr₂Ni and the stable C16 phase argue for existence of distorted C16-like structures in the amorphous alloy. In a companion paper,²² the latter group suggested that the glass is stabilized by densely packed tetrahedrons surrounded by more loosely packed polytetrahedrons without specific details of these structures. Wang *et al.*²⁵ suggested that the glass looks more like the large fcc Ti₂Ni type. In this paper, we set out to determine more specifically which kind of polytetrahedral structures give rise to form the short-range order of this weak glass-forming alloy and how these structures connect to form MRO in this system.

Our approach is to analyze the correlation of the local structure order and dynamics between the undercooled liquid and glass. We use the combination of state-of-the-art experimental techniques, *ab initio* molecular dynamics (MD) and reverse Monte Carlo (RMC) to determine the three-dimensional (3D) atomic structure for the undercooled liquid and glass of Zr₂Ni. We will show that the formation of metallic glass in this system is correlated with the slow dynamics of two specific types of Ni-centered Voronoi polyhedra (VPs) with indices of $\langle 0,2,8,1 \rangle$ and $\langle 0,2,8,2 \rangle$. These poly-

hedra have strong spatial correlation with a few less-mobile Zr-centered VPs, to form the backbone network of the metallic glass.

II. EXPERIMENTAL AND SIMULATION DETAILS

Experimental samples of Zr₂Ni metallic glass were prepared by arc-melting buttons of high-purity Zr and Ni, then rapidly cooling using a rapidly rotating Cu quench wheel. The high-energy transmission synchrotron x-ray diffraction (HEXRD) at the 6-ID-D MUCAT beamline of the Advanced Photon Source at Argonne National Laboratory was used to determine the total scattering structure factor of the glass sample at room temperature using standard methods. For the liquid measurements, electrostatic levitation techniques were combined with high-energy x-ray synchrotron methods as previously described.²⁶

The *ab initio* MD simulations were performed within density-functional theory using plane-wave basis, with the projector-augmented-wave method for core-valence-electron interactions^{27,28} and the Perdew-Wang exchange and correlation potential²⁹ as implemented in VASP code.³⁰ The cutoff energy of plane-wave basis is 270 eV. The simulations were carried out in the canonical ensemble (*NVT*) with N ose thermostats. The time step was set to be 3 fs. A cubic cell containing 99 atoms (66 Zr+33 Ni) was used with periodic boundary conditions. Only the Γ point was used to sample the supercell Brillouin zone. The average pressure of the system at each temperature was tuned to a value close to zero by changing the size of the cubic supercell. After the liquid was thermally equilibrated at 1173 K by cooling from the high-temperature liquid at 2500 K (well above the melting temperature 1293 K),²⁶ an additional 14 000 MD steps were performed to collect the atomic trajectories to study the structure and dynamics of the liquid. The glass state at 300 K was obtained by further cooling from the undercooled liquid with a cooling rate of 0.025 K/step. The structural properties of the amorphous states are then calculated by performing statistical averages over 5000 MD steps at 300 K.

Although *ab initio* MD simulations can provide a great

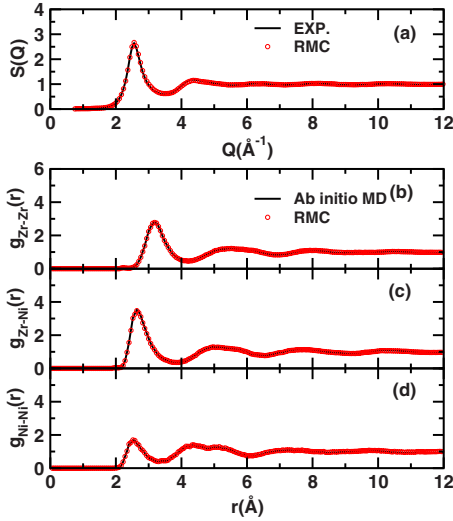


FIG. 1. (Color online) The structure model of Zr_2Ni undercooled liquid at 1173 K from the constrained RMC simulation reproduce well the structure factor $S(q)$ from experimental XRD (a) and partial PCFs from *ab initio* MD [(b), (c), and (d)].

deal of insight into the short-range structural and chemical order information in metallic liquids and glasses, 3D atomic models with several thousand atoms or more will be more useful for studying higher-order and longer-range correlations in these systems. In the present study, the RMC method^{31–33} was employed to generate the 3D atomic configurations with 25 002 atoms and periodic boundary conditions for the undercooled liquid and glass alloys. In contrast to previous RMC simulations,^{18,20} which only adopt either $S(q)$ or $G(r)$ as a constraint and thus produce rather disordered structures, we simultaneously fit the experimentally measured $S(q)$, the partial pair-correlation functions (PCFs) and the distribution of Honeycutt-Anderson (HA) indices³⁴ obtained from the *ab initio* MD simulations in our RMC simulations to determine the more unique 3D atomic structure models for the liquid and glass alloys.

The reliability of the atomistic structures generated from our constrained RMC simulations can be seen from the comparison of structural information such as structure factor and partial PCFs obtained from the RMC simulations with those from our XRD experiments and *ab initio* MD simulations, as shown for the Zr_2Ni undercooled liquid and glass in Figs. 1 and 2, respectively. The distributions of the HA indices (not shown here) in the RMC models also exhibit similar consistency with those from *ab initio* MD simulations. Furthermore, the bond-angle distributions from the RMC models are also consistent with those from *ab initio* MD simulations, although bond-angle distributions are not used as constraints in the RMC simulation.

To check the uniqueness of the atomistic models produced by RMC method, we have performed the RMC simulations for the glass structure of Zr_2Ni using three different initial configurations with randomly generated atomic coordinates, atomic positions taken from Zr_2Ni liquid at 1173 K, and a structure with a high fraction of icosahedral short range order (ISRO) based on the $Zr_{35}Cu_{65}$ glass.³⁵ The Zr and Ni sites are randomly assigned to each atomic coordinates to achieve the

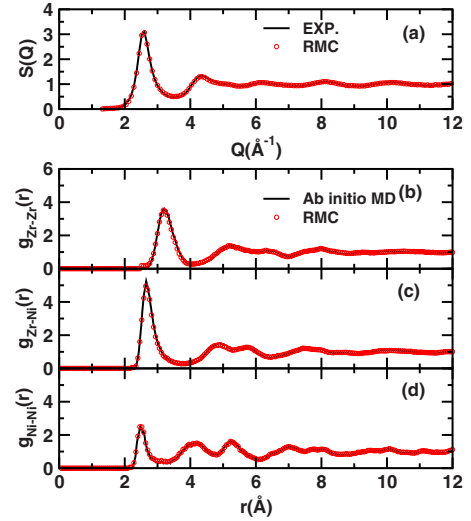


FIG. 2. (Color online) Same as in Fig. 1 for Zr_2Ni metallic glass at 300 K.

proper stoichiometry, and the atomic number density of the initial samples are adjusted to fit the density of the Zr_2Ni glass (0.053 atoms/Å³) by slightly rescaling the box size. After the RMC simulation, the resulting models obtained from different initial configurations all achieve the same goodness-of-fit as that shown in Figs. 1 and 2. We use Voronoi tessellation^{2,36} to check the similarities of the three final structures obtained by starting from random, liquid, and ISRO-rich initial configurations. Each Voronoi polyhedron is defined by a set of indices $\langle n_3, n_4, n_5, \dots \rangle$, where n_i denotes the number of i -edged bounded faces of the polyhedron around a center atom. The fractions of various VPs in the initial liquid and ISRO-rich configurations and that in the final glass samples are plotted against that in and from the random initial model, respectively, in Figs. 3(a) and 3(b). Note that if the VP distributions are exactly identical in the three samples, all the points should lie exactly on the diagonal line. As one can see from Fig. 3(b), all the points are very close to the diagonal line, indicating that the resulting atomic structures from the three very different initial configurations display very similar VP distributions after remarkable agreement has been achieved with the experimental and *ab initio* MD data through our constrained RMC fitting. In the following, the final configurations resulting from the randomly initialized atomic coordinations are used for the structural analysis of the 3D atomic packing.

III. SHORT-RANGE ORDER

Using the partial PCFs $g_{ij}(r)$ from the *ab initio* MD or RMC simulations, the partial coordination numbers (N_{ij}) can be readily calculated. The results obtained for Zr_2Ni glass at 300 K are given in Table I. For comparison, previously reported values from experiments are also included. Good agreement between the simulation and experiment can be found for N_{Zr-Ni} , N_{Ni-Zr} , and N_{Ni-Ni} when comparing the experimental results of Ref. 20. For the case of N_{Zr-Zr} , the value from the simulation is somewhat less than the experimental

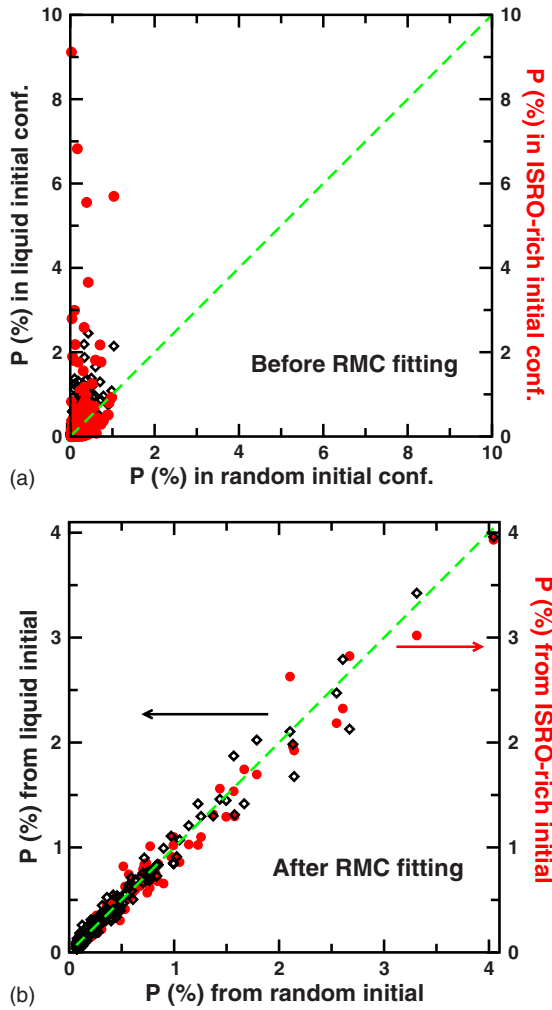


FIG. 3. (Color online) (a) Scatter plot of the total fractions of various VP types in different initial configurations vs that in the random initial configurations. (b) Scatter plot of the total fractions of various VP types from different initial configurations vs that from the random initial configuration. The empty diamond and solid circle correspond to the fraction distribution resulting from the liquid Zr₂Ni and an ISRO-rich model, respectively. Identical distribution should lie on the dashed line.

results by Lima *et al.*²⁰ and Mizoguchi *et al.*,³⁷ but very close to the value reported by Liu *et al.*²⁴ Considering some ambiguities in determining the positions of first minima of $g_{ij}(r)$ in the calculation of coordination numbers and the possible experimental errors, this discrepancy is acceptable.

SRO in the metallic glass can also be characterized by the populations of various VPs in the samples. Figure 4(b) shows

TABLE I. The nearest-neighbor coordination numbers, $N(A-B)$ (number of B atoms around A atoms), for Zr₂Ni metallic glasses.

	$N(\text{Zr-Zr})$	$N(\text{Zr-Ni})$	$N(\text{Ni-Zr})$	$N(\text{Ni-Ni})$
This work	9.97	4.08	8.16	1.70
Ref. 24 (EXAFS)	9.9	2.5	4.4	1.0
Ref. 20 (XRS)	11.6	4.2	8.4	1.3
Ref. 37 (ND)	11.0	4.8	8.6	3.3

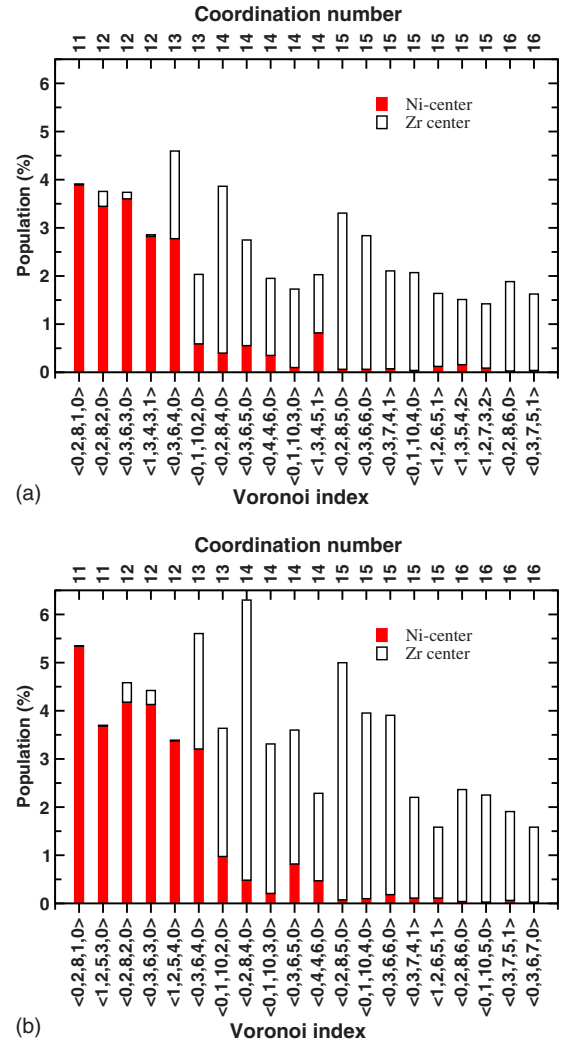


FIG. 4. (Color online) Fractions of the 20 most frequent VPs in (a) Zr₂Ni undercooled liquid at 1173 K and (b) glasses at 300 K, develop upon undercooling from the liquid due to their thermodynamic stability, normalized by total Zr and Ni atoms for Zr- and Ni-centered VPs, respectively.

the population of the 20 most abundant polyhedra in the Zr₂Ni metallic glass from our RMC simulations. For comparison, the counterpart of the undercooled liquid is also shown in Fig. 4(a). The polyhedra indices are arranged in the order of increasing coordination number (CN). Most VPs with CN less than 13 are Ni-centered while those with CN larger than 13 are Zr centered due to the larger atomic size of Zr. It is interesting to note from Fig. 4(b) that the population of the icosahedral polyhedron (Voronoi index $\langle 0,0,12,0 \rangle$)³⁸ is not within the top 20 most abundant VPs in this glass. In fact, the population of the $\langle 0,0,12,0 \rangle$ VP is only 0.52% in this glass system. The most abundant VPs in this system are $\langle 0,2,8,4 \rangle$ and $\langle 0,2,8,5 \rangle$ which are mainly Zr centered, and $\langle 0,3,6,4 \rangle$ which is a mixture of Ni- and Zr-centered VPs. For Ni-centered VPs, $\langle 0,2,8,1 \rangle$, $\langle 0,2,8,2 \rangle$, and $\langle 0,3,6,3 \rangle$ are the most common ones.

IV. KEY STRUCTURE UNITS FOR GLASS FORMATION AND THE NATURE OF MRO

Experimental studies and atomistic simulations of the liquid-to-glass transition consistently indicate the development of structural order on the scale of 5–20 Å upon cooling from high-temperature liquids, coinciding with a significant slowing down of the undercooled liquid’s dynamics until structural arrest is reached.³⁹ Therefore, we propose two criteria to identify which VP types are instrumental in glass formation: (1) the candidate VP must show a significant increase in their population upon cooling from the liquid; (2) and those atoms and their associated VP types which have the lowest mean-square-displacement (MSD) are most likely responsible for development of slow dynamics in the undercooled liquid. Identification of the VP types that meet the first criterion is a straightforward comparison of the populations in the undercooled and glass samples. To identify the VPs that give rise to the slow dynamics in the system, we have analyzed those atoms that have the lowest mobility at the time interval corresponding to the maximum of non-Gaussian parameter,⁴⁰ which corresponds to the late stage of β relaxations or a time right before the starting of α relaxations.^{41,42} At this time interval, the distribution of atomic motion in the undercooled liquid is most heterogeneous. This time interval is about 3 ps for the undercooled liquid Zr_2Ni at 1173 K and will be increased rapidly if the liquid is further undercooled. It would be interesting to study the dynamics in glass-forming liquids at the deep undercooled condition where the β relaxation time approaches the nanosecond time scale but this is beyond the capabilities of the computational resources used in this study. Nevertheless, even at the less deep undercooled liquid at 1173 K, the structure precursors and slow dynamics relevant to the glass formation in this system have already emerged. We calculate the MSD of each atoms in the undercooled liquid during this time interval from *ab initio* MD simulations and determine the 10% of slowest atoms according their MSD values. The VP types for these 10% slowest atoms is then compared to their population in the whole undercooled liquid sample (i.e., enhanced population in the 10% slowest atoms), thus identifying the slowest diffusing VPs.

In Fig. 5(a), the population changes from undercooled liquid to glass vs the enhanced population in the top 10% of the slowest atoms relative to that in the whole liquid sample are presented for the 50 most prevalent VPs. The VPs toward the upper-right quarter of this plot are more likely to contribute to glass formation since they have a larger population increase from the undercooled liquid to glass and at the same time exhibit slower dynamics. Among the Ni-centered VPs, those with the $\langle 0,2,8,1 \rangle$ and $\langle 0,2,8,2 \rangle$ indices have slower dynamics and a large population increase upon cooling. Several types of Zr-centered VPs, i.e., $\langle 0,2,8,4 \rangle$, $\langle 0,2,8,5 \rangle$, $\langle 0,1,10,4 \rangle$, and $\langle 0,1,10,3 \rangle$, also appear on the right-hand side. These four types of Zr-centered VPs also have a strong tendency to be the nearest neighbors of the $\langle 0,2,8,1 \rangle$ and $\langle 0,2,8,2 \rangle$ VPs (i.e., on the first shell of $\langle 0,2,8,1 \rangle$ and $\langle 0,2,8,2 \rangle$ clusters), as one can see from Fig. 5(b) where the percentage change in population for various VPs on the first shell of $\langle 0,2,8,1 \rangle$ and $\langle 0,2,8,2 \rangle$ clusters relative to that in

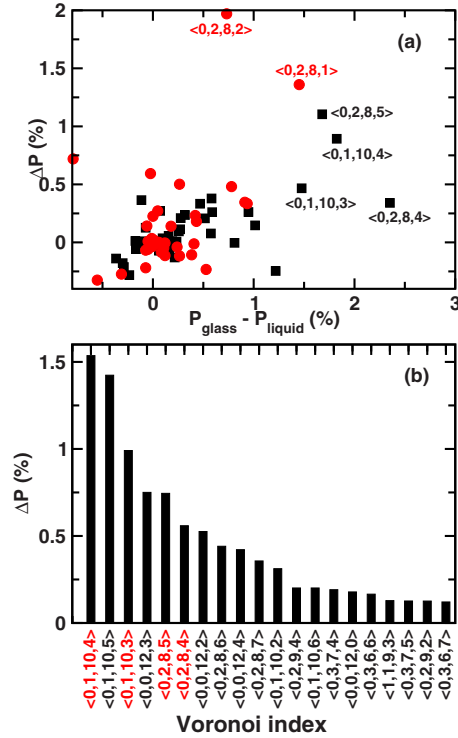


FIG. 5. (Color online) (a) The population changes from undercooled liquid to glass ($P_{glass} - P_{liquid}$) vs the population difference between the 10% of slowest diffusing atoms and the whole liquid sample (ΔP) for the most prevalent VPs. Red circles and black squares correspond to Zr- and Ni-centered VP indices, respectively. Only the top six are labeled. (b) The population differences of the various VP types on the first shell of the $\langle 0,2,8,1 \rangle$ and $\langle 0,2,8,2 \rangle$ clusters and in the whole glass sample.

the whole sample is plotted. It is therefore very plausible to designate all the Ni-centered $\langle 0,2,8,1 \rangle$ and $\langle 0,2,8,2 \rangle$ clusters and the four types of Zr-centered clusters that are on the first shell of the $\langle 0,2,8,1 \rangle$ and the $\langle 0,2,8,2 \rangle$ VP as the backbone of the glass. As the liquid is cooled down, the population of these clusters increased. The relatively slow dynamics of these clusters will promote the glass formation in this system.

In order to gain some insights into the MRO in this amorphous system, we have analyzed the network formed by the center atoms of $\langle 0,2,8,1 \rangle$, $\langle 0,2,8,2 \rangle$, and the four related Zr-centered VPs. There are 791 Ni-centered $\langle 0,2,8,1 \rangle$ and $\langle 0,2,8,2 \rangle$ clusters consisting of 7281 atoms in our RMC generated glass structure of 25 002 atoms. The fraction of the atoms involved in $\langle 0,2,8,1 \rangle$ and $\langle 0,2,8,2 \rangle$ clusters is therefore about 29%. The connectivity analysis of the $\langle 0,2,8,1 \rangle$ and $\langle 0,2,8,2 \rangle$ Ni-centered VPs is shown in Fig. 6(a) (gridded bars). The majority of the $\langle 0,2,8,1 \rangle$ and $\langle 0,2,8,2 \rangle$ clusters in this glass system have a connectivity of 0 (i.e., isolated). Therefore, $\langle 0,2,8,1 \rangle$ and $\langle 0,2,8,2 \rangle$ VPs alone in the Zr_2Ni system cannot form a good network although they do satisfy the two glass-forming criteria proposed above. However, as we already noticed in Fig. 5, there are several types of Zr-centered VPs (i.e., $\langle 0,2,8,4 \rangle$, $\langle 0,2,8,5 \rangle$, $\langle 0,1,10,3 \rangle$, and $\langle 0,1,10,4 \rangle$) exhibit stronger correlation with the Ni-centered $\langle 0,2,8,1 \rangle$ and $\langle 0,2,8,2 \rangle$ VPs, in both spatially and dynami-

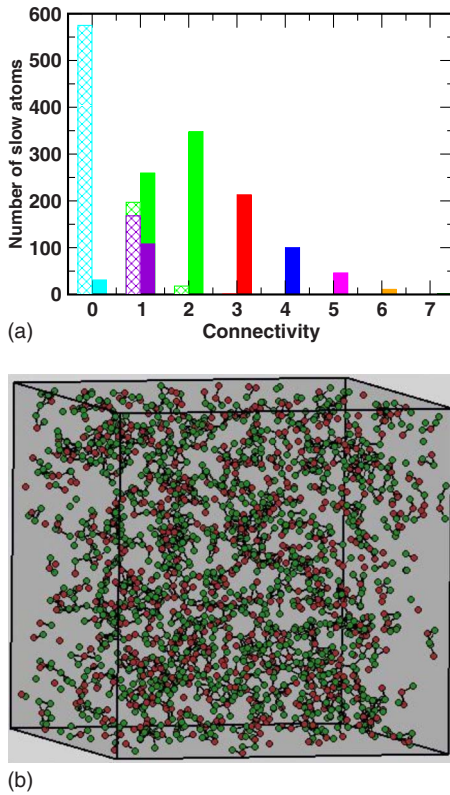


FIG. 6. (Color online) Spatial connectivity of the slow VPs. (a) shows the distribution of the number of nearest-neighbor connections among the Ni central atoms of $\langle 0,2,8,1 \rangle$ and $\langle 0,2,8,2 \rangle$ VPs (grided bars) and that plus their neighboring Zr atoms belonging to the center atoms of $\langle 0,2,8,4 \rangle$, $\langle 0,2,8,5 \rangle$, $\langle 0,1,10,3 \rangle$, and $\langle 0,1,10,4 \rangle$ VPs (solid bars). The purple and green colors denote the portion of atoms belonging to dimers or at the end of chains and branches, respectively. (b) Spatial distribution of the Ni central atoms of $\langle 0,2,8,1 \rangle$ and $\langle 0,2,8,2 \rangle$ VPs (red balls) with their neighboring Zr atoms belonging to the center atoms of $\langle 0,2,8,4 \rangle$, $\langle 0,2,8,5 \rangle$, $\langle 0,1,10,3 \rangle$, and $\langle 0,1,10,4 \rangle$ VPs (green balls).

cally. Therefore, it is plausible to expect that $\langle 0,2,8,1 \rangle$ and $\langle 0,2,8,2 \rangle$ VPs can form a strong solidlike backbone network for the glass with the help of these Zr-centered VPs. By adding the four types of related Zr-centered VPs that are nearest neighbors of $\langle 0,2,8,1 \rangle$ and $\langle 0,2,8,2 \rangle$ VPs, the number of VPs and the number of atoms involved in solidlike backbone network are 2041 and 13 691, respectively. The number of atoms involved in the solidlike backbone amount to $\sim 54.8\%$ of atoms in the system which would be large enough to enforce the glass formation under a suitable cooling rate. As shown in Figs. 6(a) and 6(b), when these associated Zr-centered VPs are included, the connectivity of the solidlike backbone network improved dramatically. However, it is not clear what the minimum percentage of the atoms in the backbone is needed in order to form a system spanning cluster, and how the glass formability of the system is quantitatively related to this percentage. These will be the issues for further investigations.

We further estimate the dimensionality d of this network from the relation $N_d \sim L^d$,⁴³ where N_d is the total number of nodes in the connected network and L is a characteristic

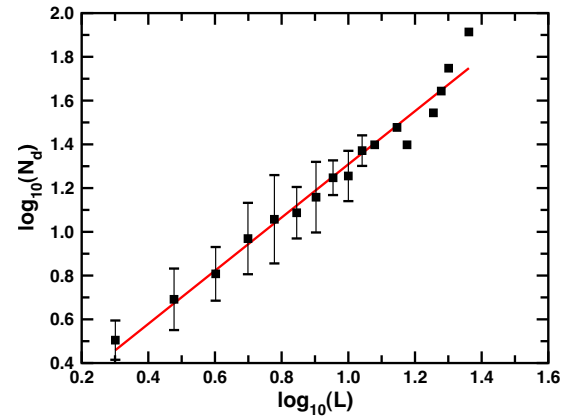


FIG. 7. (Color online) $\log_{10}(N_d)$ versus $\log_{10}(L)$ of the network consisting of Ni central atoms of $\langle 0,2,8,1 \rangle$ and $\langle 0,2,8,2 \rangle$ VPs and their neighboring Zr atoms belonging to the center atoms of $\langle 0,2,8,4 \rangle$, $\langle 0,2,8,5 \rangle$, $\langle 0,1,10,3 \rangle$, and $\langle 0,1,10,4 \rangle$ VPs. Topological dimensionality analysis is carried out for each group of connected center atoms. N_d is the total number of nodes in each connected network and L is the characteristic length of the network and defined as the maximum among the topologically shortest path between all node pairs in the network.

length of the network and defined as the maximum among the topologically shortest path between all node pairs. A linear dependence of $\log_{10}(N_d)$ on $\log_{10}(L)$ with a slope of $d \approx 1.14$ is obtained as shown in Fig. 7, indicating that the network is stringlike. Such stringlike backbone network might be the key factor leading to the glass formation in this system by freezing out relaxation processes to prevent crystallization.

V. SUMMARY

We have developed a systematic scheme to identify the essential local structure characteristics that are responsible for the glass formation in metallic glass systems. We proposed two criteria to identify the cluster types that are responsible for the glass formation: (1) the candidate VP must show a significant increase in their population upon cooling from the liquid; (2) and those atoms and their associate VP types exhibit slow dynamics in the undercooled liquid. We showed that the formation of metallic glass in Zr_2Ni system can be attributed to the slow dynamics of two special types of Ni-centered VPs with the Voronoi index of $\langle 0,2,8,1 \rangle$ and $\langle 0,2,8,2 \rangle$ as well as some associated Zr-centered VPs. These nonicosahedral clusters form a stringlike backbone network for the metallic glass and results in a heterogeneous glass structure consisting of the solidlike backbone network immersed in a liquidlike matrix.

ACKNOWLEDGMENTS

Work at Ames Laboratory was supported by the U.S. Department of Energy, basic Energy Sciences, including a grant of computer time at the National Energy Research Supercomputing Center (NERSC) in Berkeley, under Contract No. DE-AC02-07CH11358.

- ¹J. D. Bernal, *Nature (London)* **185**, 68 (1960).
- ²J. L. Finney, *Proc. R. Soc. London, Ser. A* **319**, 479 (1970).
- ³P. H. Gaskell, *Nature (London)* **276**, 484 (1978).
- ⁴D. B. Miracle, *Nature Mater.* **3**, 697 (2004).
- ⁵H. W. Sheng, W. K. Luo, F. M. Alamgir, J. M. Bai, and E. Ma, *Nature (London)* **439**, 419 (2006).
- ⁶S. Y. Wang, C. Z. Wang, M. Z. Li, L. Huang, R. T. Ott, M. J. Kramer, D. J. Sordelet, and K. M. Ho, *Phys. Rev. B* **78**, 184204 (2008).
- ⁷K. F. Kelton, G. W. Lee, A. K. Gangopadhyay, R. W. Hyers, T. J. Rathz, J. R. Rogers, M. B. Robinson, and D. S. Robinson, *Phys. Rev. Lett.* **90**, 195504 (2003).
- ⁸H. L. Peng, M. Z. Li, W. H. Wang, C. Z. Wang, and K. M. Ho, *Appl. Phys. Lett.* **96**, 021901 (2010).
- ⁹L. Huang, C. Z. Wang, S. G. Hao, M. J. Kramer, and K. M. Ho, *Phys. Rev. B* **81**, 014108 (2010).
- ¹⁰G. W. Lee, A. K. Gangopadhyay, T. K. Croat, T. J. Rathz, R. W. Hyers, J. R. Rogers, and K. F. Kelton, *Phys. Rev. B* **72**, 174107 (2005).
- ¹¹F. C. Frank, *Proc. R. Soc. London, Ser. A* **215**, 43 (1952).
- ¹²P. J. Steinhardt, D. R. Nelson, and M. Ronchetti, *Phys. Rev. Lett.* **47**, 1297 (1981).
- ¹³H. Reichert, O. Klein, H. Dosch, V. Honkimaki, T. Lippmann, and G. Reiter, *Nature (London)* **408**, 839 (2000).
- ¹⁴T. Schenk, D. Holland-Moritz, V. Simonet, R. Bellissent, and D. M. Herlach, *Phys. Rev. Lett.* **89**, 075507 (2002).
- ¹⁵W. K. Luo, H. W. Sheng, F. M. Alamgir, J. M. Bai, J. H. He, and E. Ma, *Phys. Rev. Lett.* **92**, 145502 (2004).
- ¹⁶F. Paul and R. Frahm, *Phys. Rev. B* **42**, 10945 (1990).
- ¹⁷K. Ohsaka, S. K. Chung, and W. K. Rhim, *Acta Mater.* **46**, 4535 (1998).
- ¹⁸T. Fukunaga, K. Itoh, T. Otomo, K. Mori, M. Sugiyama, H. Kato, M. Hasegawa, A. Hirata, Y. Hirotsu, and A. C. Hannon, *Intermetallics* **14**, 893 (2006).
- ¹⁹M. J. Kramer, M. Xu, Y. Y. Ye, D. J. Sordelet, and J. R. Morris, *Metall. Mater. Trans. A* **39**, 1847 (2008).
- ²⁰J. C. de Lima, D. Raoux, J. M. Tonnerre, D. Udron, K. D. Machado, T. A. Grandi, C. E. M. de Campos, and T. I. Morrison, *Phys. Rev. B* **67**, 094210 (2003).
- ²¹L. Yang, S. Yin, X. D. Wang, Q. P. Cao, J. Z. Jiang, K. Saksl, and H. Franz, *J. Appl. Phys.* **102**, 083512 (2007).
- ²²X. J. Liu, G. L. Chen, X. Hui, T. Liu, and Z. P. Lu, *Appl. Phys. Lett.* **93**, 011911 (2008).
- ²³J. Saida, M. Kasai, E. Matsubara, and A. Inoue, *Ann. Chim. (Paris)* **27**, 77 (2002).
- ²⁴X. J. Liu, X. D. Hui, H. Y. Hou, T. Liu, and G. L. Chen, *Phys. Lett. A* **372**, 3313 (2008).
- ²⁵H. R. Wang, Y. L. Gao, Y. F. Ye, Z. Q. Shi, and X. Y. Teng, *J. Alloys Compd.* **349**, 140 (2003).
- ²⁶S. G. Hao, M. J. Kramer, C. Z. Wang, K. M. Ho, S. Nandi, A. Kreyszig, A. I. Goldman, V. Wessels, K. K. Sahu, K. F. Kelton, R. W. Hyers, S. M. Canepari, and J. R. Rogers, *Phys. Rev. B* **79**, 104206 (2009).
- ²⁷P. E. Blöchl, *Phys. Rev. B* **50**, 17953 (1994).
- ²⁸G. Kresse and D. Joubert, *Phys. Rev. B* **59**, 1758 (1999).
- ²⁹Y. Wang and J. P. Perdew, *Phys. Rev. B* **44**, 13298 (1991).
- ³⁰G. Kresse and J. Furthmüller, *Comput. Mater. Sci.* **6**, 15 (1996).
- ³¹R. L. McGreevy, *J. Phys.: Condens. Matter* **13**, R877 (2001).
- ³²D. A. Keen and R. L. McGreevy, *Nature (London)* **344**, 423 (1990).
- ³³L. Pusztai and G. Toth, *J. Chem. Phys.* **94**, 3042 (1991).
- ³⁴J. D. Honeycutt and H. C. Anderson, *J. Phys. Chem.* **91**, 4950 (1987).
- ³⁵M. Z. Li, C. Z. Wang, S. G. Hao, M. J. Kramer, and K. M. Ho, *Phys. Rev. B* **80**, 184201 (2009).
- ³⁶V. A. Borodin, *Philos. Mag. A* **79**, 1887 (1999).
- ³⁷T. Mizoguchi, S. Yoda, N. Akutsu, S. Yamada, J. Nishioka, T. Suemasa, and N. Watanabe, in *Rapidly Quenched Metals* (Elsevier, New York, 1985), p. 483.
- ³⁸F. C. Frank and J. S. Kasper, *Acta Crystallogr.* **11**, 184 (1958).
- ³⁹For a review, see, e.g., G. A. Appignanesi and J. A. Rodriguez Fris, *J. Phys.: Condens. Matter* **21**, 203103 (2009).
- ⁴⁰A. Rahman, *Phys. Rev.* **136**, A405 (1964).
- ⁴¹Y. Q. Cheng, H. W. Sheng, and E. Ma, *Phys. Rev. B* **78**, 014207 (2008).
- ⁴²M. Z. Li, C. Z. Wang, M. I. Mendeleev, and K. M. Ho, *Phys. Rev. B* **77**, 184202 (2008).
- ⁴³J. Feder, *Fractals* (Plenum, New York, 1988).